JGR Oceans

RESEARCH ARTICLE
10.1029/2020JC016305

The Impact of the Amundsen Sea Freshwater Balance on Ocean Melting of the West Antarctic Ice Sheet

David T. Bett[1,2], Paul R. Holland[1], Alberto C. Naveira Garabato[2], Adrian Jenkins[1,3], Pierre Dutrieux[4], Satoshi Kimura[5], and Andrew Fleming[1]

[1]British Antarctic Survey, Cambridge, UK, [2]Ocean and Earth Sciences, University of Southampton, Southampton, UK, [3]Geography and Environmental Sciences, Northumbria University, Newcastle, UK, [4]Lamont-Doherty Earth Observatory, Columbia University, Palisades, NY, USA, [5]Japan Agency for Marine-Earth Science and Technology, Yokosuka, Japan

Abstract The Amundsen Sea has the highest thinning rates of ice shelves in Antarctica. This imbalance is caused by changes in ocean melting induced by warm Circumpolar Deep Water (CDW) intrusions. The resulting changing freshwater balance could affect the on-shelf currents and mixing. However, a clear understanding of the sources and sinks of freshwater in the region is lacking. Here we use a model of the Amundsen Sea, with passive freshwater tracers, to investigate the relative magnitudes and spatial distributions of the different freshwater components. In the surface layer and as a depth average, all freshwater tracer concentrations are of comparable magnitude, though on a depth average, sea ice and ice shelf are largest. The total freshwater tracer distribution is similar to that of the ice-shelf tracer field. This implies a potential for ice-shelf meltwater feedbacks, whereby abundant ice-shelf meltwater alters the ocean circulation and stratification, affecting melting. Ice-shelf and sea-ice freshwater fluxes have the largest interannual variability. The effect of including grounded icebergs and iceberg freshwater flux are studied in detail. The presence of icebergs increases CDW intrusions that reach the base of ice shelves. This suggests another possible feedback mechanism, whereby more icebergs induce greater ice-shelf melting and hence more icebergs. However, the strength of this potential feedback is dependent on poorly constrained sea-ice model parameters. These results imply that poorly constrained parameters relating to the ocean freshwater balance, such as those relating to icebergs and sea ice, impact predictions for melting of the West Antarctic Ice Sheet.

Plain Language Summary The Amundsen Sea in Antarctica is an important region for understanding future sea-level rise from the West Antarctic Ice Sheet, as the region's ice shelves (the floating extension of ocean terminating glaciers) are thinning due to changes in ocean melting. This could affect the amount of freshwater in the Amundsen Sea, possibly affecting ocean currents. In order to understand the distribution of freshwater from different sources (snowfall, ice-shelf melting, iceberg melting, and sea-ice melting) we use a specialized ocean model. This model shows that freshwater from all different sources have comparable magnitudes, though ice-shelf and sea-ice sources are largest. The fact that ice-shelf meltwater is an important component implies a potential feedback in the system, whereby more ice-shelf melting could alter ocean currents, and thereby cause more melting. We also investigated the effect of icebergs that ground on a seabed ridge. Icebergs increase the amount of warm water that reaches ice shelves. This provides a potential for another feedback, where more icebergs increase ice-shelf melting, thereby producing more icebergs. These results imply that poorly known aspects of freshwater sources can impact predictions for future sea-level rise contributions from the West Antarctic.

Key Points:
- Sea ice and ice shelves provide the strongest freshwater fluxes in the Amundsen Sea, with the largest interannual variability
- Parameterized icebergs affect oceanic heat content at ice shelves, with a strong potential for ice-shelf meltwater and iceberg feedbacks
- Poorly constrained parameters relating to the freshwater balance may impact predictions for melting of the West Antarctic Ice Sheet

Supporting Information:
- Supporting Information S1

Correspondence to:
D. T. Bett,
d.bett@bas.ac.uk

Citation:
Bett, D. T., Holland, P. R., Naveira Garabato, A. C., Jenkins, A., Dutrieux, P., Kimura, S., & Fleming, A. (2020). The impact of the Amundsen Sea freshwater balance on ocean melting of the West Antarctic Ice Sheet. *Journal of Geophysical Research: Oceans*, *125*, e2020JC016305. https://doi.org/10.1029/2020JC016305

Received 9 APR 2020
Accepted 21 AUG 2020
Accepted article online 26 AUG 2020

1. Introduction

The Antarctic Ice Sheet has been persistently losing mass during the satellite era. It is estimated to have added ~7.6 mm to sea-level rise (1992–2017), with most of the rise coming from ice loss from the West Antarctic Ice Sheet totaling ~6.5 mm over the same period (Shepherd et al., 2018). The largest ice-shelf thickness losses occurs in the Amundsen and Bellingshausen seas, with these two regions combined providing over 85% of the total ice-shelf volume loss from West Antarctica (1994–2012) (Paolo et al., 2015). This is thought to be due to the ocean forcing applied to these ice shelves (Shepherd et al., 2004).

In the Amundsen Sea, warm and saline modified Circumpolar Deep Water (CDW) resides below colder and fresher Winter Water (WW). The CDW resides off the continental shelf in the Antarctic Circumpolar Current (ACC) and intrudes onto the shelf via troughs in the bathymetry (Jacobs et al., 1996). These troughs extend to the base of ice shelves, enabling the modified CDW to cause high melt rates (Walker et al., 2007).

Observations taken on the continental shelf in the Amundsen Sea show that this modified CDW layer exhibits a strong seasonality and interannual variability with, for example, a pronounced cooling in 2012 (Dutrieux et al., 2014). This interannual variability is linked to winds over the continental shelf break affecting the ocean surface stresses over trough mouths (Kimura et al., 2017; Thoma et al., 2008). Eastward wind anomalies barotropically strengthen the shelf break undercurrent (Walker et al., 2013) and thus enhance CDW transport onto the shelf (Assmann et al., 2013), with these wind anomalies being linked to interannual tropical Pacific variability (Dutrieux et al., 2014; Steig et al., 2012). It is possible for the West Antarctic Ice Sheet to be stable on longer timescales even with decadally varying oceanic forcing (Snow et al., 2017). However, superimposed on the natural variability of the winds is evidence of an anthropogenic increase of eastward wind anomalies, suggesting that warm CDW anomalies may become more prevalent and could possibly have led to the imbalance of the glaciers in the region (Holland et al., 2019). Although the role of winds affecting the CDW flux onto the continental shelf appears to be the dominant driver of the interannual variability of oceanic heat content (OHC) on the shelf, there is evidence also for the role of sea-ice growth in modulating OHC (St-Laurent et al., 2015; Webber et al., 2017).

With the Amundsen Sea hosting several rapidly melting and thinning ice shelves, it is also known for its abundance of icebergs. There is a semipermanent feature of grounded icebergs on a seabed feature we refer to as Bear Ridge (Mazur et al., 2017, 2019). These grounded icebergs will henceforth be referred to as the Bear Ridge Icebergs (BRI). Their location is shown in Figure 1a and are shown in the satellite images in Figures 1d and 1f and supporting information Movie S1. The presence of BRI forms the Amundsen Sea Polynya (ASP) to its west (Figure 1c), by blocking the westward movement of sea ice (St-Laurent et al., 2015, 2017). A recent study suggests more icebergs grounded on this topographic feature during the period 2006 to 2012 compared to observations in 1997 (Mazur et al., 2019), possibly due to an increase in iceberg calving from local ice shelves. An initial study into the effects of the grounded BRI on CDW intrusions has been conducted by Nakayama, Timmermann, Schröder, and Hellmer (2014), in which static sea ice was used to simulate the fast ice induced by grounded BRI. This study found that BRI had little effect under weakly biased atmospheric forcing, but ocean conditions in Pine Island Bay were warmer with the BRI when a cold-biased forcing was used. This suggests that grounded BRI may act as a buffer to CDW modulation in anomalously cold years.

The change in ice discharge from ice shelves in the Amundsen Sea will change the poorly known freshwater balance of the region. This increased input of freshwater into the region could affect the on-shelf currents and mixing, due to density being strongly controlled by salinity in the polar regions (Gill, 1982). This could have many effects, including regional sea-level rise (Rye et al., 2014) and a freshening of the downstream Ross Sea (Jacobs & Giulivi, 2010).

Regan et al. (2018) examined the freshwater balance of the nearby Bellingshausen Sea by adding tracers to track the influence of each source of freshwater in a regional ocean model. There, it was found that sea ice dominates the seasonal freshwater cycle, all freshwater sources make comparable contributions to the annual mean, and sea ice and precipitation dominate the interannual variability. Studies of ice-shelf freshwater alone have been performed in the Amundsen Sea (Kimura et al., 2017; Nakayama et al., 2017; Nakayama, Timmermann, Rodehacke, et al., 2014), with ice-shelf meltwater found to have highest concentrations close to the coast, setting up the strong westward geostrophic coastal current (Jourdain et al., 2017). This agrees with observations, as ice-shelf meltwater can be traced in the Amundsen Sea with its highest concentrations similarly close to the coast (Biddle et al., 2017; Nakayama et al., 2013).

In this study we use a high-resolution regional model of the Amundsen Sea, with freshwater tracers, to investigate the relative magnitudes and spatial distributions of the different freshwater components: ice-shelf melt, sea-ice melt/freeze, parameterized iceberg melt, and the combined effect of precipitation and evaporation. An analysis of the different freshwater components' interannual variability is conducted. Grounded icebergs in the region are also considered, and their effect on the interannual variability of OHC reaching ice shelves in the region is investigated.

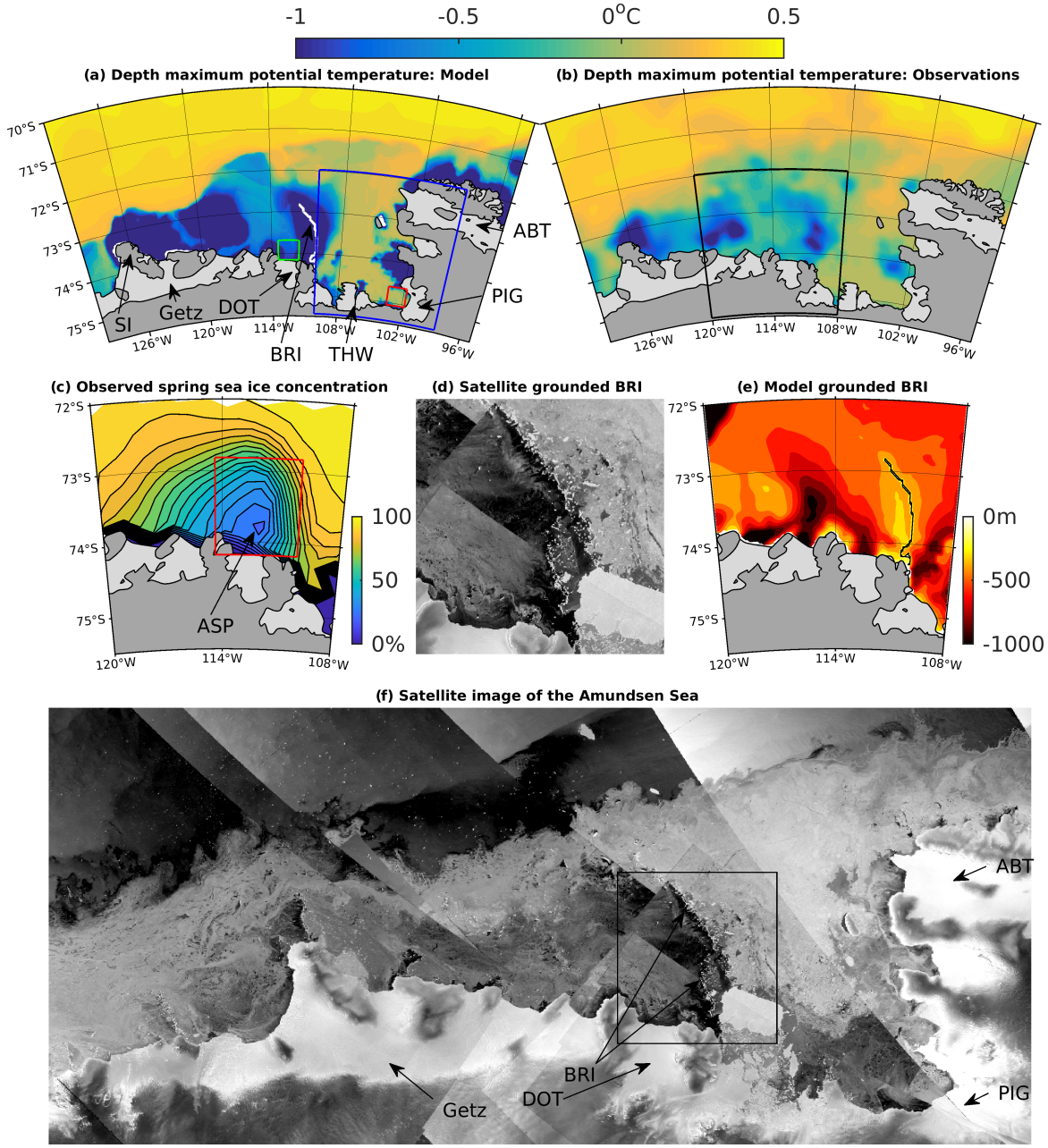

Figure 1. Depth maximum climatological subsurface potential temperature (1994–2012, but using only observational available years) from (a) model and (b) observations (Dutrieux et al., 2014). The black box in (b) shows the area in (c) and (e). (c) Spring satellite observations of the AMSR-E sea-ice concentrations (2003–2010) (Cavalieri et al., 2014). (e) Model bathymetry with representation of grounded icebergs. (d, f) Satellite image mosaic composed of Copernicus Sentinel-1 SAR (synthetic aperture radar) data. The composite uses imagery acquired between 30 April 2017 and 6 May 2017. Image composite was processed by BAS using Google Earth Engine. The black box in (f) shows the area in (d). Key locations are shown in (a), (c), and (f), where SI = Siple Island, DOT = Dotson Ice Shelf, BRI = Bear Ridge Icebergs, THW = Thwaites Ice Shelf, PIG = Pine Island Glacier Ice Shelf, ABT = Abbot Ice Shelf, and ASP = Amundsen Sea Polynya.

2. Methods

Revision c62r of Massachusetts Institute of Technology general circulation model (MITgcm) is used, following the configuration used by Kimura et al. (2017). A longitudinal resolution of 0.1° is used, producing a latitudinal spacing ranging from ~2.8 km in the southern part of the domain to ~5.2 km at the northern end of the domain. In the vertical, a z-level coordinate system of 50 levels is used, ranging from 10 m resolution near

the top to 200 m near the bottom (reaching 5,600 m here). The model domain extends from 75.5°S to 62°S and 140°W to 80°W covering the Amundsen Sea embayment, but we will concentrate our analysis on the region extending from 75.5°S to 71.5°S and 130°W to 95°W.

Freshwater from several different sources (iceberg melt, evaporation, precipitation, sea ice, and ice-shelf meltwater) are tracked via distinct passive tracers (Regan et al., 2018). A volumetric source of tracer occurs when freshwater is added, and a volumetric sink occurs when freshwater is removed, for example, via evaporation or sea-ice growth. Such sinks can create negative tracer concentrations in the domain. Therefore, we shall consider a freshwater flux into the ocean as positive and a freshwater flux out of the ocean as negative. Only local freshwater sources are traced in the model, and therefore, freshwater entering the domain via the open boundary conditions are not traced.

Following Kimura et al. (2017), there is no explicit horizontal diffusion of salt, heat, or tracers in the model, but the vertical diffusion is parametrized by using the K-profile parameterization (KPP) scheme (Large et al., 1994). Initial conditions were interpolated onto the model grid from the World Ocean Atlas (Locarnini et al., 2013; Zweng et al., 2013). Steady climatological conditions for ocean velocity, salinity, and temperature, taken from Holland et al. (2014), are applied to the eastern, northern, and western boundaries. Using climatological boundary conditions does not capture small remotely induced variations in CDW temperature (Nakayama et al., 2018), but this temperature variation has a much smaller effect than locally induced variability of the CDW layer thickness that occurs within the region and is captured by the model. Tides are not accounted for in the model. The model is forced with ERA-Interim reanalysis forcing from 1979–2018 (Dee et al., 2011), but we regard the first 10 years as model spin-up, as it takes this long for the model to spin up from the initial conditions to the open boundary conditions.

For this study, several improvements have been made to the Kimura et al. (2017) model setup. In order to correct a long-term sea-level fall in the model the open boundary velocities were edited, and sea-ice parameters were tuned to replicate interannual variability of OHC in front of PIG. In particular, the air-ice drag coefficient is set to 0.0025, the ice-ocean drag coefficient is set and fixed to the default value of 0.0053, the demarcation ice thickness is set to the default value of 0.5 m (Hibler, 1979), and sea-ice advection uses a third-order direct-space-time flux-limited scheme. Ocean parameters were kept the same as those used by Kimura et al. (2017).

Icebergs are represented in the model via iceberg melt and the physical presence of grounded icebergs on Bear Ridge. Grounded BRI are built into the model by modifying the seabed, which is raised to the sea surface to create a "wall" along the 350 m depth contour around the shallow area north of Bear Island (Figure 1e). Fast ice surrounding the grounded BRI is not explicitly included in this study, though the sea-ice model permits sea ice to build up around the BRI. An alternative method of implementing the BRI as a 10-m-thick ice shelf was tested, allowing the ocean to flow through the BRI, but only minor differences were seen in the results (not shown). As an initial study of the influence of iceberg freshwater, iceberg melting of the numerous icebergs crossing the domain is crudely represented as a fixed freshwater flux into the ocean surface. The total flux into the domain is set to be 198 Gt/year, which is equal to the iceberg discharge in the Amundsen Sea (Depoorter et al., 2013; Rignot et al., 2013), as we assume that imported and exported icebergs compensate each other. The iceberg freshwater flux is input near the coast, tapering linearly to zero 100 km away, as iceberg-modeling studies suggest that Amundsen Sea icebergs stay close to the coast (Merino et al., 2016). The simulation including BRI, iceberg melt, and air-ice drag coefficient set to 0.0025 will henceforth be referred to as the reference case.

3. Results

3.1. Model Validation

The model broadly recreates the climatology of the modified CDW intrusions onto the continental shelf (Figure 1a), compared to observations (Figure 1b) (Dutrieux et al., 2014). However, the model is colder in the Dotson Trough compared to observations, which could be due to the shallow model bathymetry in this area compared to observations.

The model is compared to summer CTD salinity and potential temperature profiles in front of PIG (Figures 2a and 2b) and Dotson ice shelves (Figures 2c and 2d), using observational CTD profiles taken in

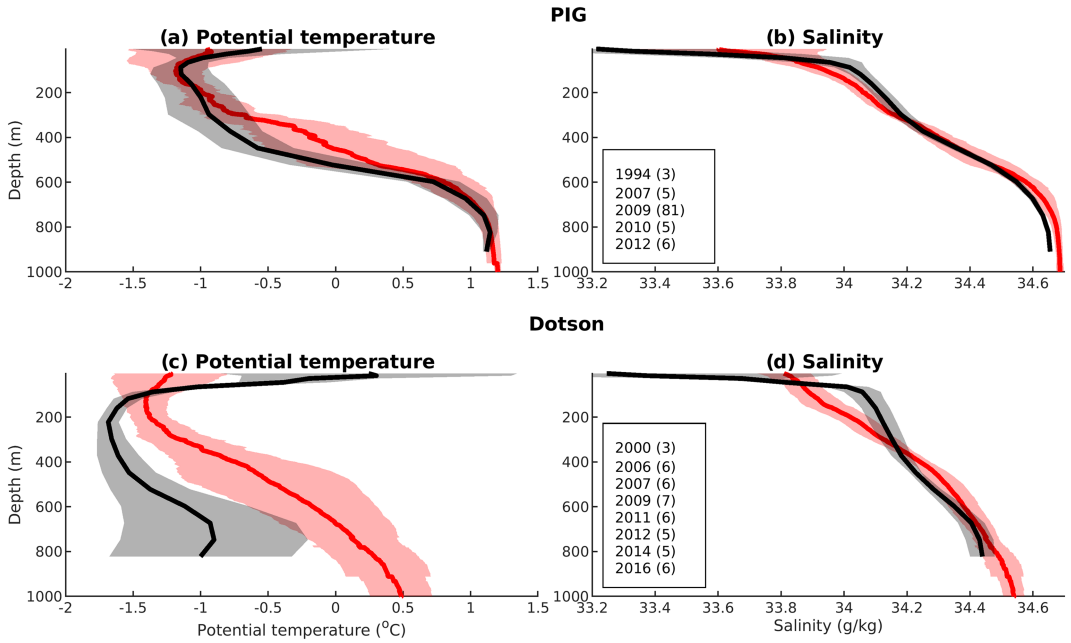

Figure 2. Observed (solid red lines) and model output from reference case (solid black line) mean profiles for salinity and potential temperature near (a, b) PIG and (c, d) Dotson ice shelves. The shaded areas represent one standard deviation of the interannual variability from the mean. CTD profiles taken from Jenkins et al. (2018) for Dotson and Dutrieux et al. (2014) for PIG, taking CTD locations that are either within the red and green boxes in Figure 1a or closer to the ice shelves. The model is sampled at the closest grid point to the individual CTD observations and at the same month and year. The number of CTD profiles for each austral summer is indicated for both regions.

the red and green boxes (Figure 1a), and closer to the ice-shelf fronts where present (Dutrieux et al., 2014; Jenkins et al., 2018). In both locations, the summer surface salinity is fresher in the model compared to observations. Near PIG Ice Shelf, the model approximately recreates observed mean salinity and temperature profiles, though with a reduced standard deviation (Dutrieux et al., 2014). However, near Dotson Ice Shelf, the model approximates the observed variation, but is too cold and unable to simulate the deepest parts of the observational casts, due to a shallow seabed data set, caused by a sparseness of data at the time of modeling. Comparisons to the detailed vertical structure of the water column are a stringent test for any model, considering the approximations caused by vertical and horizontal grid resolution and uncertain models of ocean mixing and sea ice. The model approximates ocean conditions sufficiently well for the purposes of this study.

To better visualize the interannual variability of the ocean conditions in front of these ice shelves, Figure 3 shows the potential temperature and salinity in front of PIG and Dotson ice shelves, using Hovmöller diagrams averaged over the green and red boxes in Figure 1a, with a 2 year running average applied at each depth. In front of PIG Ice Shelf, the model captures the observed colder conditions in 2000 and warm years of 2007–2010. It also features a cooler period in the mid-2010s, though this cooling is later and less intense than observed (Dutrieux et al., 2014). In front of Dotson Ice Shelf the model captures the large variability observed at the depths simulated in the model, with the model being cold in 2000 and warm approximately from 2006–2011 and cold again 2012–2016 (Jenkins et al., 2018).

Figure 4 shows the mean of the seasonal sea-ice concentrations from 2003 to 2010 for the model (panels e–h), so it can be compared to satellite observations taken from AMSR-E (panels a–d) (Cavalieri et al., 2014). The model replicates the sea-ice concentration observations well in winter and spring. However the model underpredicts sea-ice cover in the summer and autumn. The grounded BRI in the model reproduces the ASP and the higher concentrations of sea ice east of the grounded BRI in the observations.

The seasonal cycle of the sea-ice thickness for the model (Figures 4i–4l) is within the range of observations for the region (Kurtz & Markus, 2012; Worby et al., 2008), though sea-ice thickness observations have a large

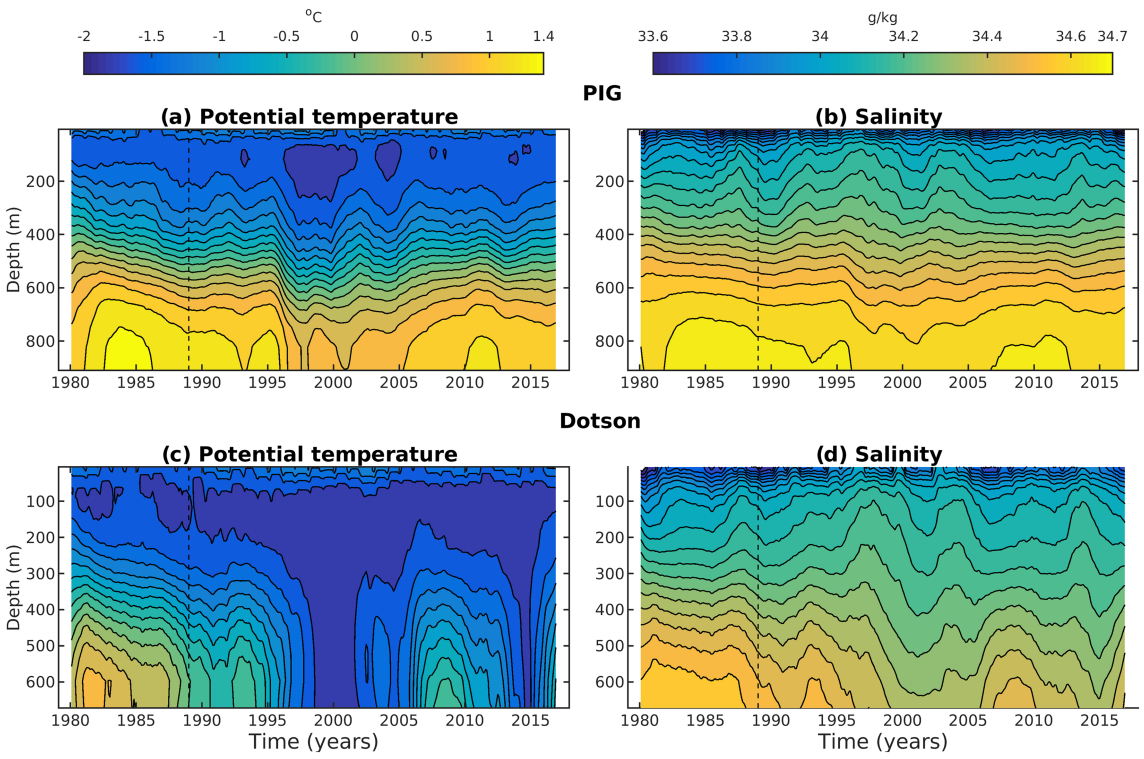

Figure 3. Hovmöller diagrams of potential temperature and salinity in front of PIG Ice Shelf (a, b) and Dotson Ice Shelf (c, d). Hovmöller diagrams are averaged over the red and green boxes shown in Figure 1a and include 10 year model spin-up. A 2 year running average is applied at each depth. Vertical black dashed lines indicate end of model spin-up period.

uncertainty. The model shows the thickest sea ice is in the winter and spring and is east of the grounded BRI and along the coast north of Abbot Ice Shelf, peaking at around 2 m in the spring. There is also substantial thickness east of Siple Island. The climatology of the ice-shelf freshwater fluxes (Figure 5e) is similar to those simulated and validated extensively in Kimura et al. (2017), with the largest ice-shelf freshwater fluxes originating from PIG and Thwaites ice shelves.

3.2. Reference Case With Tracers

Figure 5 shows the spatial distribution of the climatological model freshwater fluxes (1989–2018), excluding a 10 year model spin-up period (1979–1988), for all the different components of the freshwater balance, along with the total freshwater flux. The PmE (precipitation minus evaporation) freshwater contribution is orders of magnitude less than the other sources, with iceberg melt flux also small in comparison, with average freshwater fluxes over the continental shelf out to the 1,000 m depth contour of 1.3×10^6 and 1.3×10^{11} m^3/year, respectively. Therefore, sea-ice and ice-shelf sources are the two main climatological contributions to the freshwater budget over the continental shelf in the Amundsen Sea, with average continental shelf freshwater fluxes of -2.5×10^{11} and 3.4×10^{11} m^3/year, respectively.

The sea-ice freshwater flux climatology distribution shows a negative freshwater flux close to the coast and a positive flux in the north. This is due to sea-ice growth in the austral winter in the south and average sea-ice transport northward and sea-ice melt in the austral spring (Abernathey et al., 2016). Therefore, the Amundsen Sea shelf is a net sea-ice export region. There is particularly strong negative freshwater flux on average in the ASP and near PIG Ice Shelf, where there is strong sea-ice growth and export/divergence in the austral winter. These results agree with observations in the region finding evidence of average sea-ice export in front of PIG, with reduced or positive melting effect found further north at the shelf break (Biddle et al., 2019). In the total flux, the iceberg melt flux partially mitigates the negative fluxes of the sea ice, but there are still negative fluxes on average in the ASP and near PIG Ice Shelf. However, due to oceanic

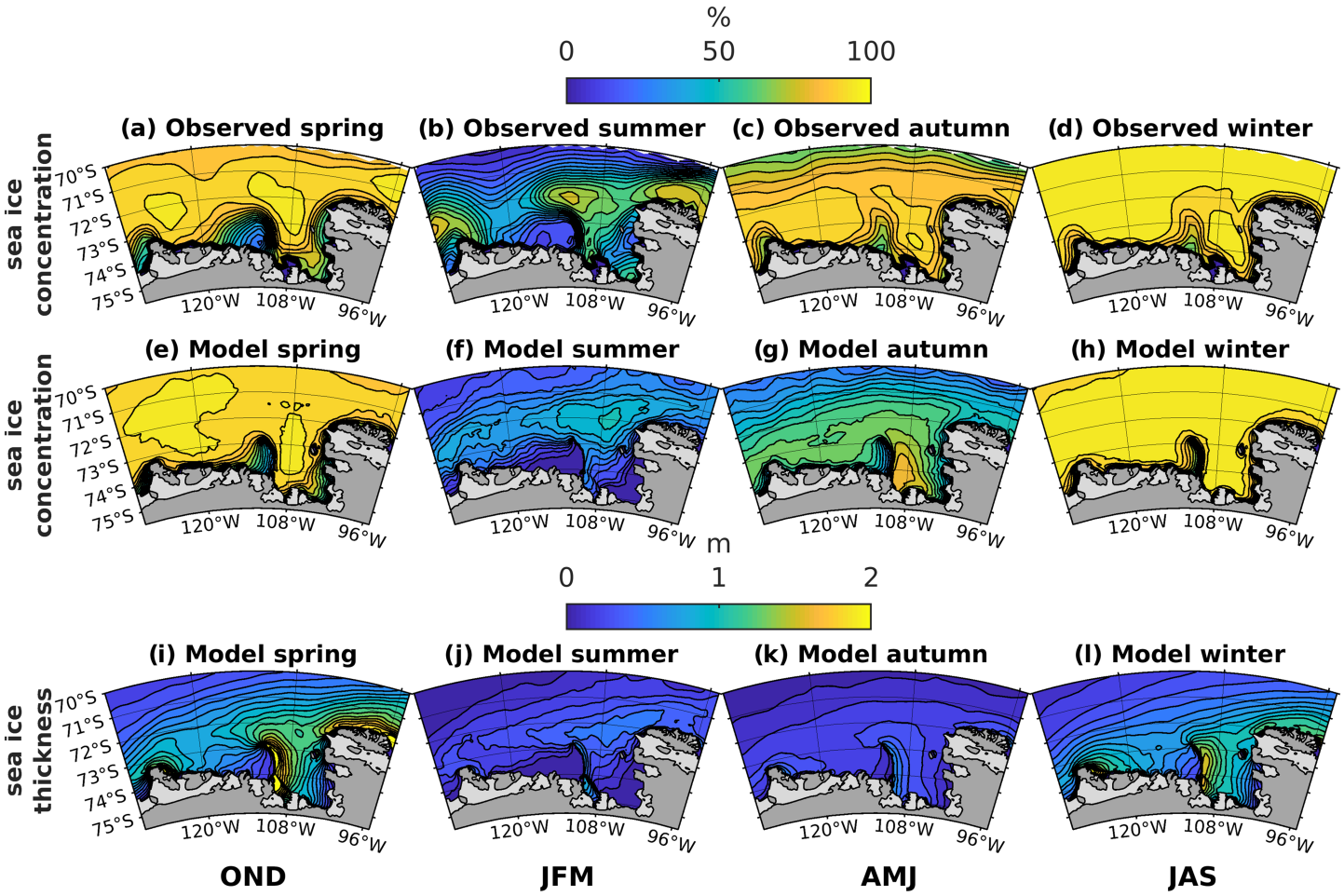

Figure 4. Climatological seasonal cycle of the satellite observations of the AMSR-E sea-ice concentrations (a–d) (Cavalieri et al., 2014). Model climatological seasonal cycle of sea-ice concentrations (e–h) and the sea-ice thickness (i–l). All averaged over the period 2003–2010.

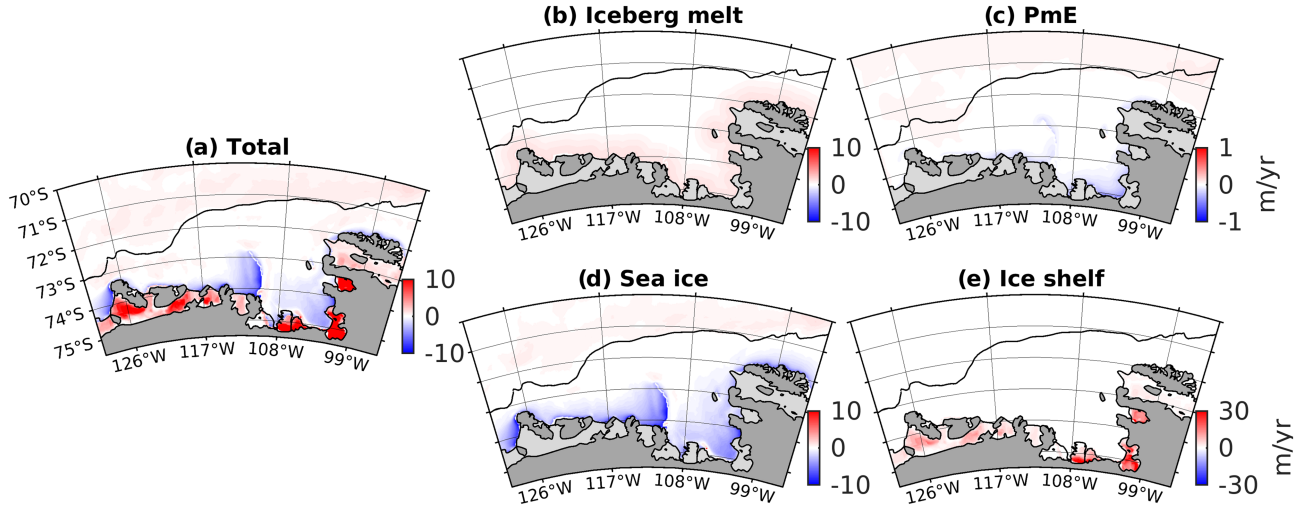

Figure 5. Climatology of freshwater fluxes (1989–2018) for (a) total freshwater, (b) iceberg melt, (c) precipitation minus evaporation (PmE), (d) sea-ice melt/freeze, and (e) ice-shelf melt. Black line represents the 1,000 m depth contour of the continental shelf break.

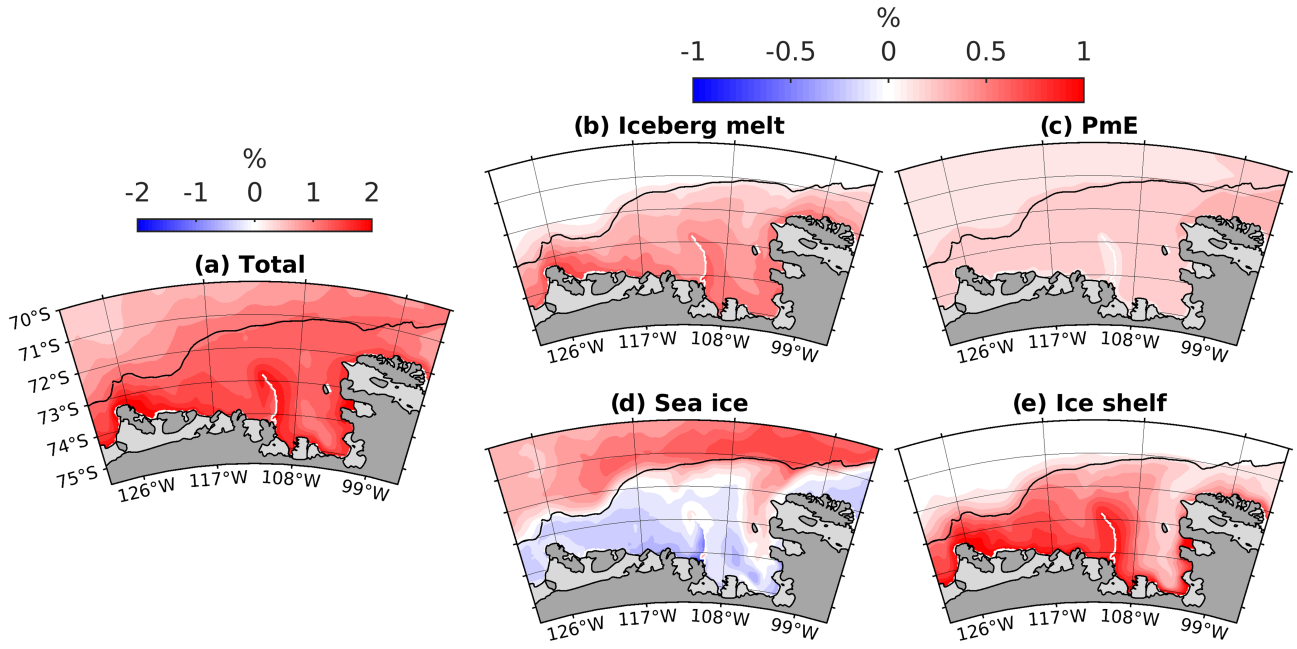

Figure 6. Climatology of surface freshwater tracer concentration (1989–2018) for (a) total freshwater, (b) iceberg melt, (c) precipitation minus evaporation (PmE), (d) sea-ice melt/freeze, and (e) ice-shelf melt. Black line represents the 1,000 m depth contour of the continental shelf break.

advection and diffusion of freshwater, we cannot determine the effect of freshwater sources by just examining the input fields; instead, we need to consider the freshwater tracers.

The climatological surface (top 10 m) tracer fields shown in Figure 6 reflect the combined processes of the spatial distribution of the flux fields and their redistribution due to oceanic advection and mixing. Off the continental shelf, positive sea-ice tracer dominates the climatology of the freshwater balance in the surface. However, on the continental shelf, all sources are of comparable importance to the surface freshwater balance, though with varying spatial distributions for the individual components. This is despite the differences in the fluxes (Figure 5), because freshwater from the larger sources (sea ice and ice shelf) is distributed over depth. Ice-shelf freshwater is released at depth, while sea-ice growth causes convection, driving its negative tracers deeper.

Ice-shelf meltwater has its highest surface concentration within the westward coastal current, which agrees with observations in the region (Biddle et al., 2017; Nakayama et al., 2013) and other modeling studies (Kimura et al., 2017). Its tracer concentration increases toward the west, as it passes an increasing number of traced ice shelves, and spreads further from the coast, though no significant amounts cross the shelf break in the surface layer. However, we are only examining local contributions to the freshwater balance, so ice-shelf meltwater from the east (Bellingshausen Sea) is not reflected in the tracers (Nakayama, Timmermann, Rodehacke, et al., 2014). Sea ice has predominantly negative surface tracer on the shelf, with the notable exception of northwest of Abbot Ice Shelf, where inflow from off the shelf brings positive sea-ice tracer on average onto the shelf. Iceberg melt and PmE both make an average positive contribution to the surface freshwater balance on the continental shelf.

The climatology of total tracer is positive in the surface for the entire region and has the highest values in the coastal current. This contrasts with the freshwater flux field shown previously (Figure 5), which has areas of negative freshwater flux, due mainly to strong negative average sea-ice freshwater flux. This negative sea-ice contribution in the surface tracer is balanced in part by the advection of ice-shelf meltwater. Furthermore negative sea-ice freshwater fluxes and evaporation cause convection, mixing negative sources of tracer down out of the surface layer.

Figure 7 shows the climatology of the depth-average freshwater tracers, calculated by taking the water column integral of tracers and then dividing by the water column height. On the continental shelf, sea ice and

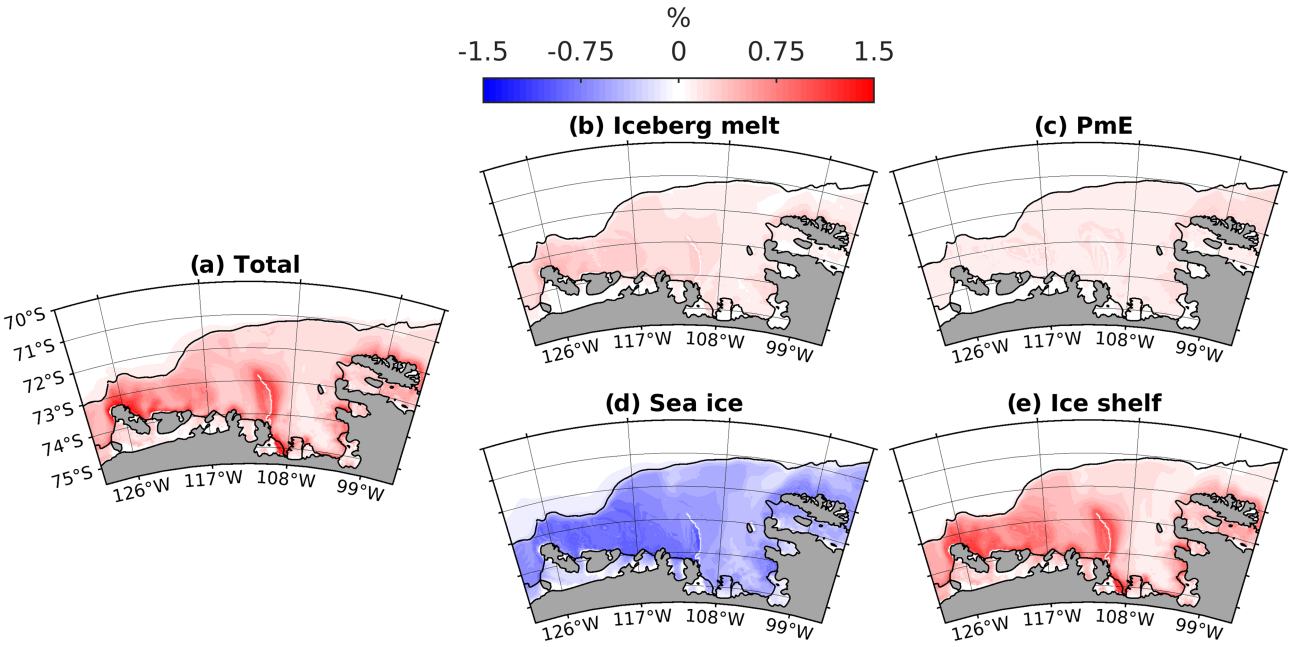

Figure 7. Climatology of depth-averaged freshwater tracer concentration (1989–2018) for (a) total freshwater, (b) iceberg melt, (c) precipitation minus evaporation (PmE), (d) sea-ice melt/freeze, and (e) ice-shelf melt. Black line represents the 1,000 m depth contour of the continental shelf break.

ice shelf are the most significant freshwater sources averaged over the water column, though iceberg melt and PmE still make notable positive contributions. Ice-shelf freshwater has the largest spatial variation, with the highest concentration near Siple Island, as this area is comparatively shallow and lies downstream of most of the region's ice shelves. Though noble gas observations of ice-shelf meltwater are very sparse, the model broadly recreates the spreading of ice-shelf meltwater observed through this technique (Biddle et al., 2019; Kim et al., 2016).

The sea-ice tracer is the only source that has a negative average value over the continental shelf. This is due to sea-ice export leading to average positive sea-ice freshwater fluxes to occur off the continental shelf and the long residence time of deep penetrating negative sea-ice tracer on the continental shelf. There is stronger negative sea-ice tracer to the west of the grounded BRI than to the east, in part due to the strong negative sea-ice freshwater fluxes in the ASP. This agrees with observations in the region (Biddle et al., 2019; Randall-Goodwin et al., 2015). Iceberg melt and PmE both have small average positive tracer concentrations, which are spatially uniform over the continental shelf. The total tracer has a very similar magnitude and distribution to the ice-shelf tracer. This implies that on average PmE and iceberg melt cancel out the negative freshwater contribution to the region from sea ice. Within ice-shelf cavities a balance between the sea-ice negative tracer and the positive ice-shelf freshwater tracer occurs, with the cavities being positive on average in the total tracer.

To summarize, sea-ice and ice-shelf processes provide the largest freshwater fluxes on average in the Amundsen Sea. Despite this, however, all freshwater tracer concentrations are of comparable magnitude, both in the surface (10 m) and on a depth average over the continental shelf. In addition, the distribution of the surface total tracer resembles that of the ice-shelf tracer, and the depth-average total tracer field is highly similar to the ice-shelf tracer.

Since the total tracer resembles the ice-shelf meltwater tracer, the melting of the ice shelves must play an important role in the circulation and stratification of the Amundsen Sea. This implies that there is a strong potential for ice-shelf meltwater feedbacks in the system. For example, an increased presence of meltwater could both accelerate currents (Jourdain et al., 2017) and stratify the ocean, potentially enhancing the transport of less-modified CDW toward the ice shelves and causing more melting and hence more meltwater. Further targeted research is required to isolate the precise nature and importance of any such feedbacks.

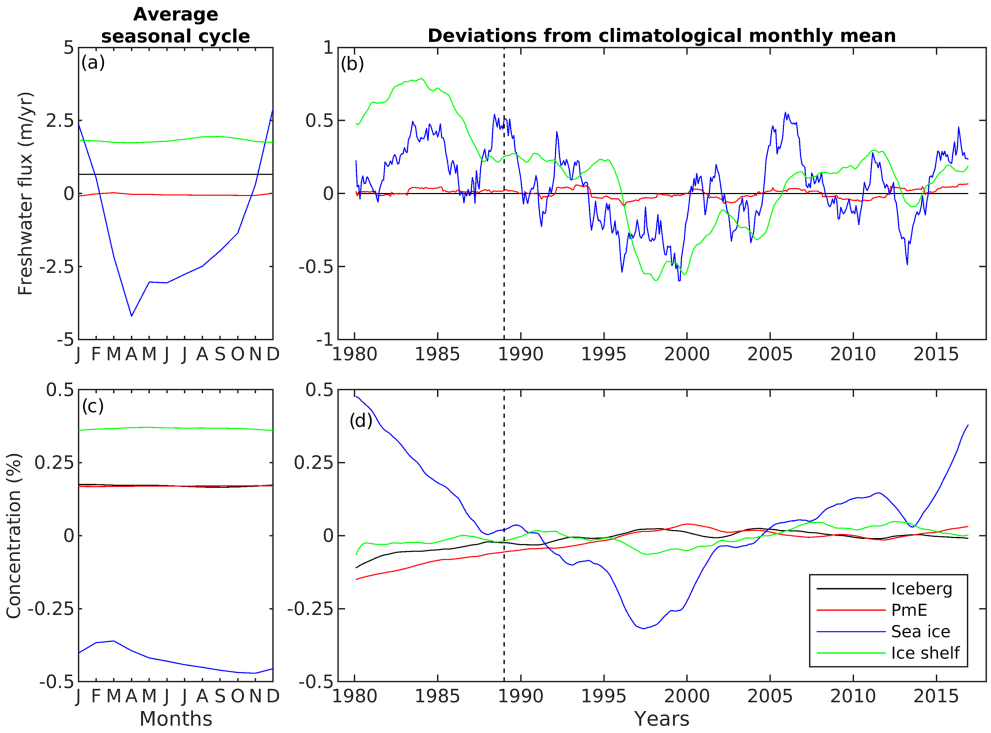

Figure 8. Eastern Amundsen Sea mean seasonal cycle for (a) freshwater component fluxes and (c) tracer concentration, along with interannual variability of (b) freshwater component fluxes and (d) tracer concentration. Fluxes and concentration are averaged over the area and volume of the blue box shown in Figure 1a, and ice-shelf meltwater flux is taken to be the combined fluxes from Thwaites and PIG ice shelves. Interannual variability is calculated as monthly anomalies from the mean seasonal cycle, with a 2 year running mean subsequently applied. Dashed vertical lines show end of model spin-up period.

3.3. Seasonality and Interannual Variability of Freshwater Sources

3.3.1. Time Series

The average seasonal cycle (1989–2018) and interannual variability of the eastern Amundsen Sea (the blue box in Figure 1a) freshwater fluxes and tracer concentration are shown in Figure 8, including the 10 year spin-up. Here, the ice-shelf freshwater flux is the combination of PIG and Thwaites ice shelves, as they are most important to the stability of the West Antarctic Ice Sheet. Sea ice has the largest seasonal freshwater flux cycle by an order of magnitude, with the sea-ice negative freshwater flux (brine rejection) peaking in April (Figure 8a). The sea ice's larger seasonal cycle is also apparent in the tracer concentration; the minimum sea-ice tracer concentration is in November (Figure 8c), when sea-ice freshwater flux becomes positive.

Sea-ice and ice-shelf freshwater fluxes have the largest interannual variability, with ice-shelf melting attaining a minimum in 1997 (Figure 8b). Examining the correlation between the interannual variability of these two freshwater fluxes, after the 10 year spin-up period, gives an $r|r|$ of ~0.35 at a lag of ice-shelf melting of 10 months (r is the correlation coefficient). This significant correlation could be due to sea-ice modulation of CDW affecting ice-shelf melt rates (St-Laurent et al., 2015). However, ice-shelf melting has a strong correlation with the volume flux of CDW through the eastern trough at the continental shelf break, with an $r|r|$ of ~0.87 at a lag of 6 months. This is in line with results of Kimura et al. (2017) for melting of PIG Ice Shelf. Thus, the interannual variability of the ice-shelf freshwater is consistent with the well-established hypothesis of the interannual variability of CDW flux onto the continental shelf. Sea-ice freshwater fluxes anticorrelate with the meridional wind anomalies over the box, with an $r|r|$ value of ~ -0.40 at zero lag. Stronger northward winds open up coastal polynyas and enhance the extraction of freshwater by freezing. The interannual variability of the sea-ice tracer concentration is an order of magnitude larger than the other tracers (Figure 8d), as negative sea-ice tracer is driven deeper in the water column, due to freezing-driven convection, and has a longer residence time at depth.

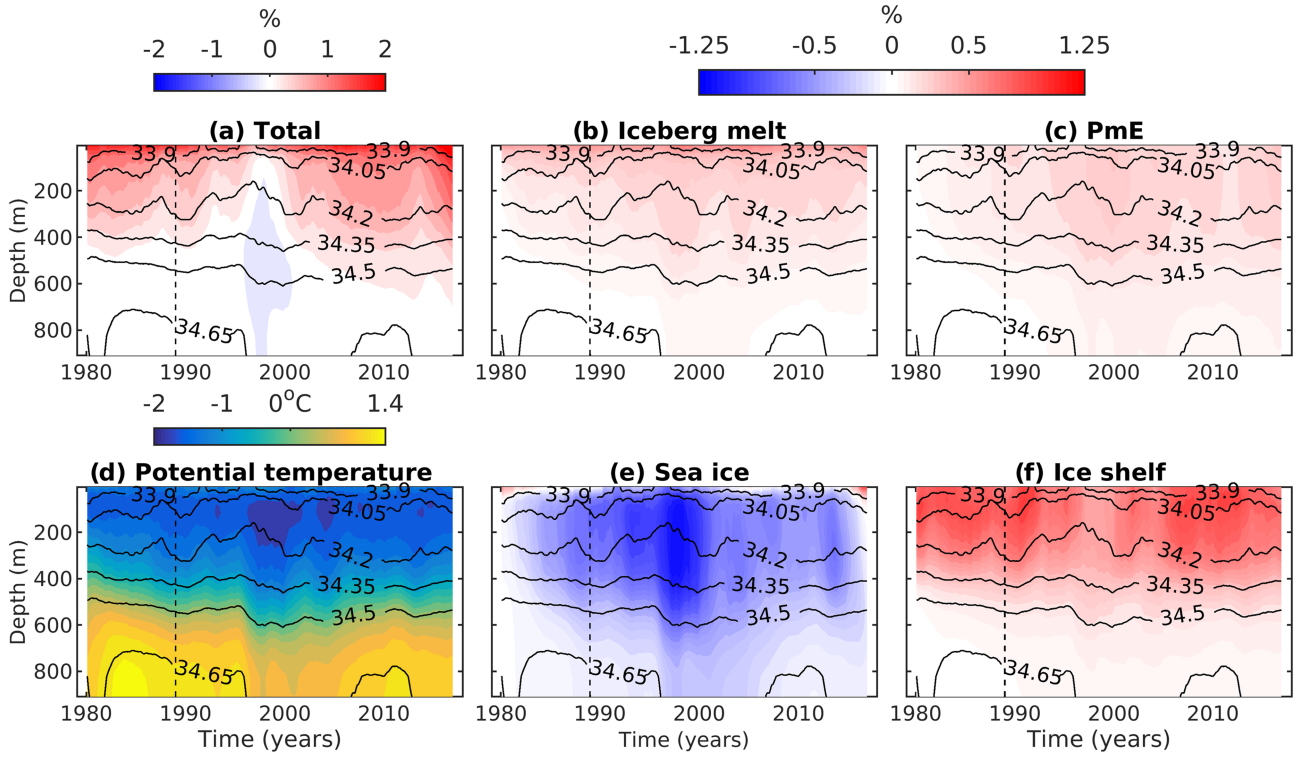

Figure 9. Hovmöller diagrams of (a) total freshwater, (b) iceberg melt, (c) precipitation minus evaporation (PmE), (d) sea-ice melt/freeze, and (e) ice-shelf melt averaged over red box in front of PIG Ice Shelf, shown in Figure 1a. Black contours indicate salinity averaged over the same area. Model spin-up of 10 years included. A 2 year running mean at each depth is applied to the tracers and the salinity to remove the seasonal cycle.

3.3.2. Vertical Distribution

We next consider the interannual variability of the vertical distribution of the total and component freshwater tracers, specifically focusing on the region in front of PIG Ice Shelf to examine the possible implications for ice-shelf melting. Figure 9 shows Hovmöller diagrams of the tracers averaged horizontally over the red box in Figure 1a. In front of PIG Ice Shelf, sea-ice and ice-shelf freshwater tracers dominate, though iceberg melt and PmE make significant positive contributions.

Negative tracer dominates over most of the water column for the sea-ice tracer, with strong interannual variability. In the period of 1997 to 2000, the sea-ice negative tracer extends down the entire water column, as intense sea-ice brine rejection mixes the surface layers down. The sea-ice tracer has a small quantity of positive tracer at the surface that displays large interannual variability, with, for example, 2017 showing significant sea-ice meltwater. The sea-ice tracer, therefore, has strong interannual variability in its concentration and in its vertical distribution.

Positive ice-shelf tracer is mostly concentrated in the top 400 m of the water column, with the highest concentrations during years of high OHC and thus higher salinity at depth. During years of low OHC, ice-shelf tracer reduces to a concentration comparable to that of PmE and iceberg melt, while sea-ice tracer becomes more negative. Therefore, in years of low OHC, the iceberg melt and PmE components are relatively more important in the freshwater balance and may mitigate freezing-driven convection in the front of PIG Ice Shelf. In contrast, during years of high OHC ice-shelf meltwater plays a significant role in stabilizing the water column against brine rejection from sea-ice growth and the modulation of the OHC.

Iceberg meltwater is concentrated near the top of the water column. However, this is most likely because iceberg meltwater is applied as a surface flux, whereas in reality, iceberg melting occurs at depth. PmE tracer is more uniform through the water column, though it still exhibits highest concentrations at the surface. The total freshwater tracer is concentrated in the surface, and its interannual variability matches that of the surface salinity. There is a strong interannual variability to the total freshwater tracer in the surface layers and

at depth. The total tracer even becomes negative at depth below 200 m, between 1997 and 2000, implying that more "local" freshwater has left these depths than entered them.

3.4. Effect of Grounded Icebergs

Nakayama, Timmermann, Schröder, and Hellmer (2014) found that grounded BRI affected ocean variability in Pine Island Bay. We extend these results by considering the role of grounded BRI over the whole Amundsen Sea, also considering the effects of iceberg meltwater, and investigating all underlying processes in detail. So far, we have chosen to include both grounded icebergs on Bear Ridge and imposed iceberg melting. These choices have an important effect on the freshwater balance and dynamics in the region. We now show these effects in four runs: "Reference," "no BRI," "no iceberg melt," and "no BRI and no iceberg melt."

The grounded BRI affect the sea-ice distribution in the region and therefore its freshwater fluxes. Figures 10a and 10b show the average winter sea-ice freshwater flux and winter sea-ice concentration and drift, in the eastern Amundsen Sea with the grounded BRI present. The strongest sea-ice freshwater fluxes out of the ocean are in the ASP and in coastal polynyas in the east; low sea-ice concentration and a high westward drift characterize these regions. Calculating the sea-ice production in the ASP over each winter (March–October) for the period 2003–2010, in the area shown by the red box in Figure 1c, gives a mean and standard deviation of $6.2 \pm 1.9 \times 10^{10}$ m^3, which is comparable to satellite-based estimates of $9 \pm 1.4 \times 10^{10}$ m^3, given the methodological error of 23% in the latter figure (Nihashi & Ohshima, 2015). Figures 10c and 10d show the same quantities but with the grounded BRI removed from the model, and Figures 10e and 10f respectively show the climatological differences (with minus without grounded BRI, and note uneven color bar).

The primary effect of the grounded BRI is to create the ASP, by blocking the flow of sea ice. This reduces sea-ice concentration to the west of the grounded BRI and significantly increases sea-ice freshwater extraction, via increased sea-ice growth. A weaker secondary effect is to increase the concentration of sea ice east of the BRI by restricting the westward export of sea ice and so reducing the eastern coastal polynyas. Therefore, the grounded BRI affect the winter sea-ice freshwater fluxes in front of both Dotson Ice Shelf and the ice shelves to the east but with opposite effects.

We now consider the effects of both the grounded BRI and iceberg meltwater on the interannual variability of OHC reaching PIG Ice Shelf and Dotson Ice Shelf, via Hovmöller diagrams of potential temperature (Figure 11). We consider the evolution of the temperature in the water column in this way as a proxy for melting. We prefer to study potential temperature because it is better observed than melting, and its depth dependence reveals the underlying processes. In front of PIG Ice Shelf for the reference case (Figure 11a), the model approximately follows the observed interannual variability of OHC reaching the PIG Ice Shelf. Removing the representation of the grounded BRI slightly lowers the thermocline and increases the depth of the WW (Figure 11b). This is due to a small increase in sea-ice brine rejection in front of the ice shelf, as the sea ice is unrestrained by the grounded BRI to the west. Convection increases, especially in the period between 1997 and 2000, thus becoming too cold at depth compared to the 2000 observations in the region (Dutrieux et al., 2014). However, removing iceberg meltwater is more significant, with WW now dominating the whole water column from 1997 and 2007 and a reduction in OHC in other years (Figure 11c). The combined effect of having neither the iceberg meltwater nor the grounded icebergs gives an even greater WW dominance in front of PIG (Figure 11d).

In front of Dotson Ice Shelf in the reference case (Figure 11e) we see a large interannual variability similar to observations (Jenkins et al., 2018). Without the presence of the grounded BRI (Figure 11f), there is a reduction in the interannual variability in WW depth, giving this simulation a reduced interannual variability compared to observations. This is due to the removal of the ASP, which leads to a strong decrease in sea-ice brine rejection, and thereby modulation of OHC. Removing iceberg melt has a very significant impact (Figure 11g), filling the whole water column with all WW after 1990 and stopping the reintroduction of warmer water even in the period of 2005 to 2010, where CDW flux onto the shelf is high in the reference case. These results demonstrate that iceberg melt is required to mitigate the convection caused by the ASP. Unexpectedly, in the case with neither iceberg aspect (Figure 11h), we observe a different interannual variability of OHC. This is because the presence of dense shelf water in the eastern Amundsen Sea in this simulation (Figure 11d) redirects modified CDW toward Dotson Ice Shelf. Comparing these results shows that both

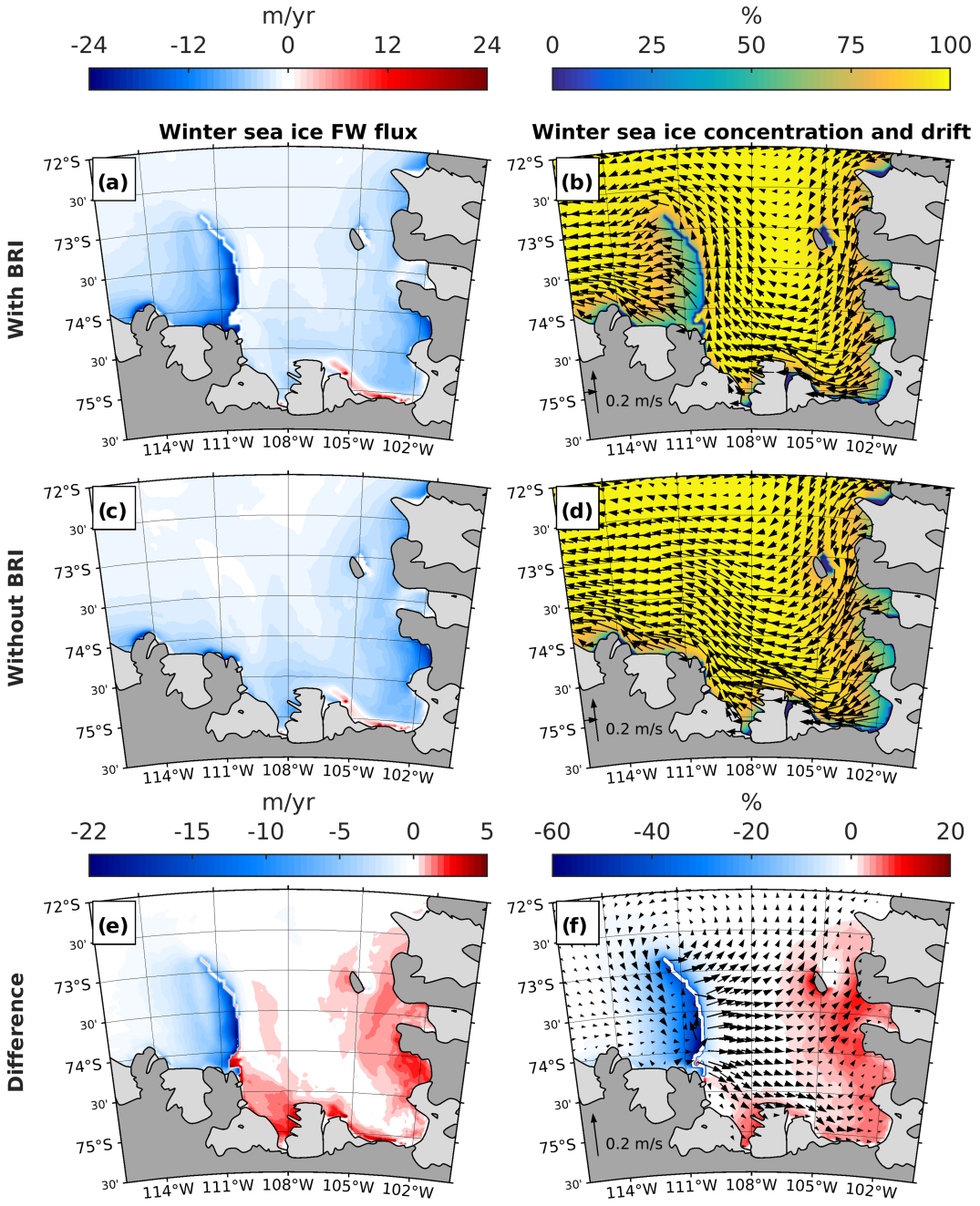

Figure 10. (a) Climatological austral winter (JAS) sea-ice freshwater flux out of the ocean (1989–2018) with grounded Bear Ridge Icebergs (BRI) and (c) without BRI. (b) Climatological winter (JAS) sea-ice concentration and drift (1989–2018) with grounded BRI and (d) without BRI. Difference in (e) winter (JAS) sea-ice freshwater flux out and (f) winter (JAS) sea-ice concentration and velocities (with minus without the representation of the grounded BRI). Note uneven color bar in (e) and (f).

aspects of icebergs are required in order to simulate the interannual variability of OHC observed at Dotson Ice Shelf.

The possible existence of a positive iceberg feedback in the freshwater system is implied by these results, for PIG and similar eastern glaciers. Both iceberg melt and the presence of grounded BRI enhance modified CDW intrusions that reach the base of the ice shelves, which would enhance ice-shelf melting east of the grounded BRI. An increase in basal melting will create an imbalance between the ice mass fluxes into and

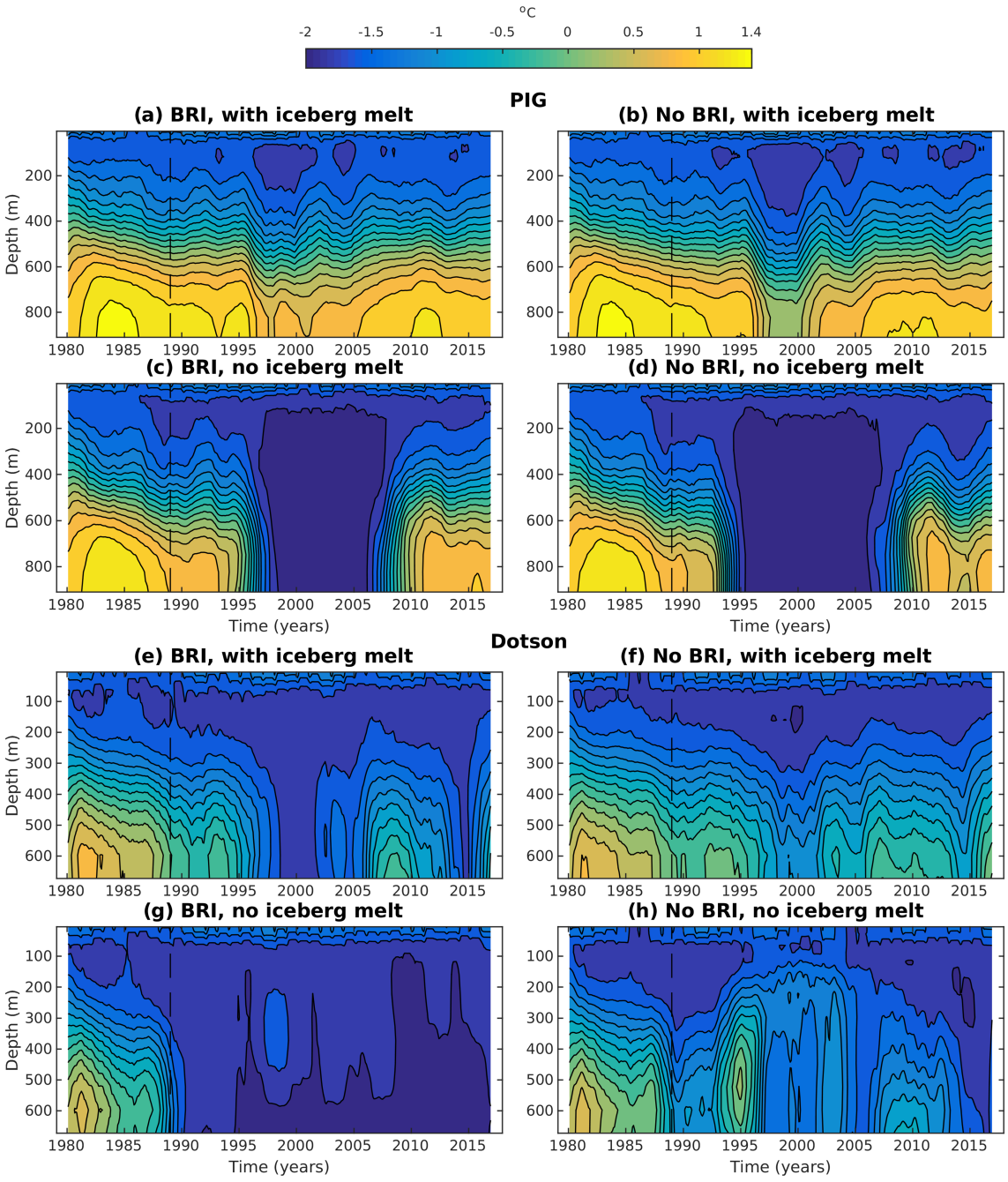

Figure 11. Hovmöller diagram of potential temperature in front of PIG Ice Shelf for (a) grounded BRI and iceberg melt, (b) no grounded BRI but with iceberg melt, (c) grounded BRI but without iceberg melt, and (d) no grounded BRI and no iceberg melt. (e–h) The same for the area in front of Dotson Ice Shelf. Hovmöller diagrams are averaged over the red and green boxes shown in Figure 1a and include 10 year model spin-up. A 2 year running average is applied at each depth. Vertical black dashed lines indicate end of model spin-up period.

out of an ice shelf, leading it to thin overall. This will cause the glacier to speed up, as thinning reduces the ice flow-restraining internal stresses within the ice shelf. The increased flow speed of the glacier will therefore lead to an increase in iceberg production, and icebergs calved from glaciers like PIG and eastern Thwaites have a drift path that leads to the Bear Ridge area (Mazur et al., 2019). Therefore, this may increase the number of icebergs grounded on Bear Ridge and increase iceberg melt in the region and so complete the potential feedback.

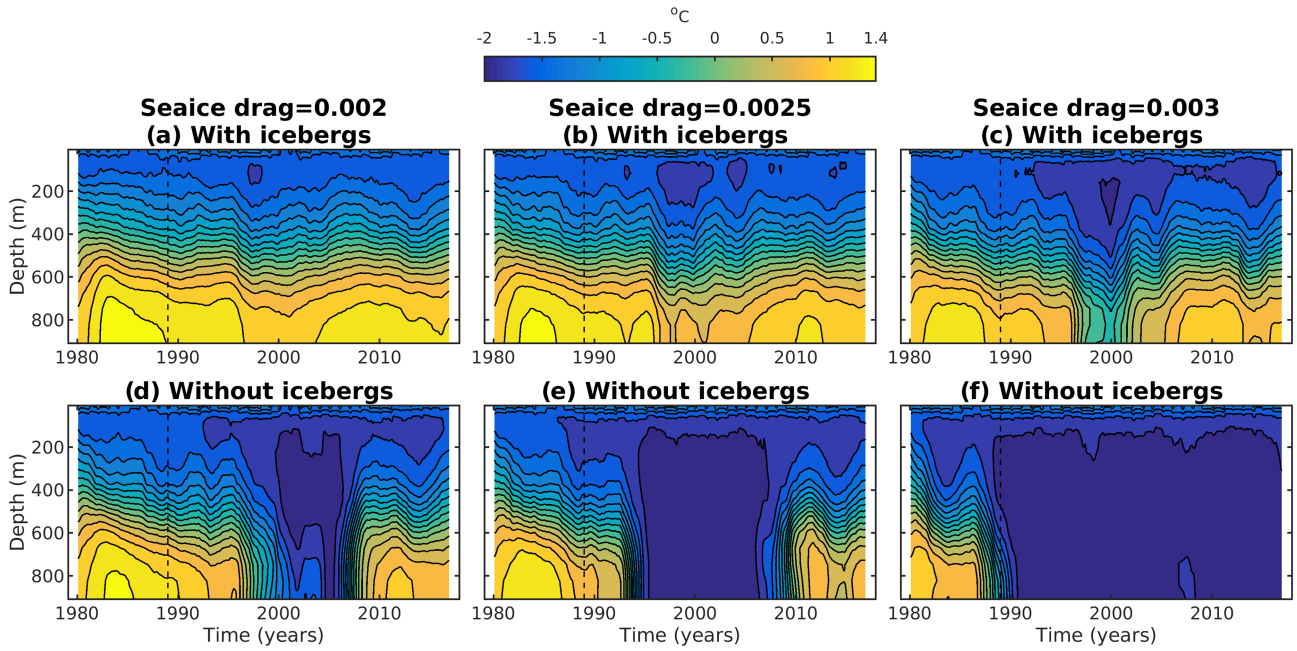

Figure 12. Potential temperature Hovmöller diagrams averaged over PIG Ice Shelf front with and without both grounded icebergs and iceberg melt for sea-ice drag parameters values of 0.002 (a, d), 0.0025 (b, e), and 0.003 (c, f), respectively. Hovmöller diagrams are averaged over the red box in Figure 1a and include 10 year model spin-up. A 2 year running mean is applied at each depth. Vertical black dashed lines indicate end of model spin-up period.

3.5. Influence of Parameter Choices

The strength of this potential freshwater feedback is dependent on the winds, since sea-ice export causes the convection that cools the OHC. In turn, this influence of the winds is dependent on the sea ice-atmosphere drag coefficient, which is a poorly constrained parameter. Some studies into the value of this parameter have been conducted for the Arctic (Petty et al., 2017), but there are few such studies in Antarctica. In our study, we have used an air-ice drag coefficient of 0.0025, which was tuned so that ocean conditions in front of PIG Ice Shelf approximately matched observations. Note that correcting this parameter is also a way to correct possible biases in ERA-Interim. To demonstrate the importance of this parameter, we now consider further simulations with different values of the air-ice drag coefficient, increasing it and decreasing it by 20% from the reference value of 0.0025 (Figure 12) and thus changing the ratio between the air-ice and ice-ocean drag coefficients.

Reducing the sea-ice drag coefficient we see a decrease in the interannual variability of OHC reaching PIG Ice Shelf and a reduction in the WW thickness (Figure 12a), due to reduced sea-ice export and formation. Conversely, increasing the drag coefficient (Figure 12c) increases the interannual variability and significantly so during the 1997–2000 period of low CDW flux onto the shelf.

Concisely, increasing this parameter increases the effect of iceberg blocking and melting. Icebergs now mean the difference between the bay being in a warm regime, with modified CDW reaching PIG Ice Shelf and therefore high ice-shelf melt, or being in a cold regime with dense shelf water formation and low ice-shelf melt. This is because with increased drag the wind moves sea ice faster, increasing local freshwater extraction via an enlargement of coastal polynyas and more rapid sea-ice export from the region. Thus, iceberg melt and the grounded BRI become more important to the freshwater balance to mitigate drag-induced changes and stop a tipping point of dense shelf water being reached, so that warm modified CDW continues to reach ice shelves like PIG.

We conclude that the strength of our proposed feedback is dependent upon the rate of sea-ice export. Note that this parameter sensitivity study can be considered as a crude wind sensitivity study, with an increase in the sea-ice drag parameter being comparable to the occurrence of stronger winds over the region. This comparison is imperfect however, as increasing this parameter is analogous to increasing only wind strength, not direction, and only over sea ice.

4. Conclusions

This study uses a numerical model of the Amundsen Sea with freshwater tracers and a representation of grounded BRI to determine the freshwater balance of the region. The results show that sea-ice and ice-shelf freshwater fluxes are climatologically the strongest in the region. In the surface (10 m) and on a depth average, however, all sources make important contributions to the climatological freshwater balance. The total freshwater tracer in the surface resembles the ice-shelf tracer, and the total freshwater tracer field is highly similar to the ice-shelf tracer on a depth average as well. This implies that there is the potential for ice-shelf meltwater feedbacks in the Amundsen Sea, since the presence of meltwater affects the ocean currents and stratification that control melting. For example, an increased presence of meltwater could both accelerate currents and stratify the ocean, potentially enhancing the transport of less-modified CDW toward the ice shelves.

Sea ice dominates the freshwater seasonal cycle. However, both the sea-ice and ice-shelf freshwater fluxes have the largest interannual variability. Sea-ice freshwater flux anomalies negatively correlate with the meridional wind anomalies, and similarly to other studies, eastern ice-shelf freshwater anomalies correlate strongly with CDW flux onto the continental shelf. Analysis of the freshwater balance in front of the PIG Ice Shelf reveals that there is a large interannual variability of the total freshwater tracer, due mainly to the strong interannual variability of the sea-ice and ice-shelf tracers. This implies that other freshwater sources like iceberg melt become relatively more important to the freshwater balance when ice-shelf meltwater flux is low.

The grounded BRI affect sea-ice distribution and drift. Their presence increases freshwater extraction west of the grounded icebergs due to the formation of the ASP, and decreases it to the east, with the reduction of eastern coastal polynyas. The combination of the grounded BRI and iceberg melt influences the interannual variability of OHC reaching the ice shelves, with effects that are different between the two cases on either side of the grounded BRI (e.g., Dotson compared with PIG). Both iceberg blocking and melting are required to recreate the interannual variability of the modified CDW reaching these ice shelves.

These results suggest a further possible positive feedback mechanism, whereby more iceberg melting increases modified CDW intrusions that reach the base of eastern ice shelves like PIG and therefore induce greater ice-shelf melting. This causes the ice shelves to thin and thus speed up, hence producing more icebergs. However, the strength of this feedback is dependent on the modeled sea-ice growth and export, which depends on the poorly constrained sea ice-atmosphere drag parameter. In a parameter study, we find that varying this parameter by 20% has a significant control over the strength of the feedback. Therefore, poorly constrained parameters relating to the freshwater balance, like those relating to icebergs and sea-ice structure, will impact predictions for melting of the West Antarctic Ice Sheet.

This study is limited by the idealized representations of grounded BRI and iceberg melt. The closely balanced nature of the freshwater components found here emphasizes the need for a more realistic representation of icebergs and fast ice to be developed for future modeling studies. Moreover, the dependency of the potential iceberg feedback on the poorly constrained sea ice-atmosphere drag coefficient highlights the need for advancing our understanding of sea ice around the Antarctic margins.

Data Availability Statement

The model output underlying the figures and calculations in this paper is available through the UK Polar Data Centre (https://doi.org/10.5285/8AD04D77-6A41-419A-B0D7-18EEE743BF26).

Acknowledgments

This work was supported by the Natural Environment Research Council (Grant NE/L002531/1). A. C. N. G. was supported by the Royal Society and the Wolfson Foundation. The authors thank the two anonymous reviewers for their careful reading of our manuscript and their constructive and helpful comments and suggestions.

References

Abernathey, R. P., Cerovecki, I., Holland, P. R., Newsom, E., Mazlo, M., & Talley, L. D. (2016). Water-mass transformation by sea ice in the upper branch of the Southern Ocean overturning. *Nature Geoscience*, *9*(8), 596–601. https://doi.org/10.1038/ngeo2749

Assmann, K. M., Jenkins, A., Shoosmith, D. R., Walker, D. P., Jacobs, S. S., & Nicholls, K. W. (2013). Variability of Circumpolar Deep Water transport onto the Amundsen Sea continental shelf through a shelf break trough. *Journal of Geophysical Research: Oceans*, *118*, 6603–6620. https://doi.org/10.1002/2013JC008871

Biddle, L. C., Heywood, K. J., Kaiser, J., & Jenkins, A. (2017). Glacial meltwater identification in the Amundsen Sea. *Journal of Physical Oceanography*, *47*(4), 933–954. https://doi.org/10.1175/JPO-D-16-0221.1

Biddle, L. C., Loose, B., & Heywood, K. J. (2019). Upper ocean distribution of glacial meltwater in the Amundsen Sea, Antarctica. *Journal of Geophysical Research: Oceans*, *124*, 6854–6870. https://doi.org/10.1029/2019JC015133

Cavalieri, D., Markus, T., & Comiso, J. C. (2014). AMSR-E/Aqua daily L3 12.5 km brightness temperature, sea ice concentration and snow depth polar grids. Version 3 for 2006–2011. Boulder, CO: NASA DAAC at the Natl. Snow and Ice Data Cent. https://doi.org/10.5067/AMSR-E/AE_SI12.003

Dee, D. P., Uppala, S. M., Simmons, A. J., Berrisford, P., Poli, P., Kobayashi, S., et al. (2011). The ERA-Interim reanalysis: Configuration and performance of the data assimilation system. *Quarterly Journal of the Royal Meteorological Society*, *137*(656), 553–597. https://doi.org/10.1002/qj.828

Depoorter, M. A., Bamber, J. L., Griggs, J. A., Lenaerts, J. T. M., Ligtenberg, S. R. M., van den Broeke, M. R., & Moholdt, G. (2013). Calving fluxes and basal melt rates of Antarctic ice shelves. *Nature*, *502*(7469), 89–92.

Dutrieux, P., de Rydt, J., Jenkins, A., Holland, P. R., Ha, H. K., Lee, S. H., et al. (2014). Strong sensitivity of Pine Island ice-shelf melting to climatic variability. *Science*, *343*(6167), 174–178. https://doi.org/10.1126/science.1244341

Gill, A. E. (1982). *Atmosphere-ocean dynamics* (1st ed., Vol. 30). New York: Academic Press.

Hibler, W. D. III (1979). A dynamic thermodynamic sea ice model. *Journal of Physical Oceanography*, *9*(4), 815–846. https://doi.org/10.1175/1520-0485(1979)009<0815:ADTSIM>2.0.CO;2

Holland, P. R., Bracegirdle, T. J., Dutrieux, P., Jenkins, A., & Steig, E. J. (2019). West Antarctic ice loss influenced by internal climate variability and anthropogenic forcing. *Nature Geoscience*, *12*(9), 718–724. https://doi.org/10.1038/s41561-019-0420-9

Holland, P. R., Bruneau, N., Enright, C., Losch, M., Kurtz, N. T., & Kwok, R. (2014). Modeled trends in Antarctic sea ice thickness. *Journal of Climate*, *27*(10), 3784–3801. https://doi.org/10.1175/JCLI-D-13-00301.1

Jacobs, S. S., & Giulivi, C. F. (2010). Large multidecadal salinity trends near the Pacific–Antarctic continental margin. *Journal of Climate*, *23*(17), 4508–4524. https://doi.org/10.1175/2010JCLI3284.1

Jacobs, S. S., Hellmer, H. H., & Jenkins, A. (1996). Antarctic ice sheet melting in the Southeast Pacific. *Geophysical Research Letters*, *23*(9), 957–960. https://doi.org/10.1029/96GL00723

Jenkins, A., Shoosmith, D., Dutrieux, P., Jacobs, S., Kim, T. W., Lee, S. H., et al. (2018). West Antarctic Ice Sheet retreat in the Amundsen Sea driven by decadal oceanic variability. *Nature Geoscience*, *11*(10), 733–738. https://doi.org/10.1038/s41561-018-0207-4

Jourdain, N. C., Mathiot, P., Merino, N., Durand, G., le Sommer, J., Spence, P., et al. (2017). Ocean circulation and sea-ice thinning induced by melting ice shelves in the Amundsen Sea. *Journal of Geophysical Research: Oceans*, *122*, 2550–2573. https://doi.org/10.1002/2016JC012509

Kim, I., Hahm, D., Rhee, T. S., Kim, T. W., Kim, C.-S., & Lee, S. (2016). The distribution of glacial meltwater in the Amundsen Sea, Antarctica, revealed by dissolved helium and neon. *Journal of Geophysical Research: Oceans*, *121*, 1654–1666. https://doi.org/10.1002/2015JC011211

Kimura, S., Jenkins, A., Regan, H., Holland, P. R., Assmann, K. M., Whitt, D. B., et al. (2017). Oceanographic controls on the variability of ice-shelf basal melting and circulation of glacial meltwater in the Amundsen Sea Embayment, Antarctica. *Journal of Geophysical Research: Oceans*, *122*, 10,131–10,155. https://doi.org/10.1002/2017JC012926

Kurtz, N. T., & Markus, T. (2012). Satellite observations of Antarctic sea ice thickness and volume. *Journal of Geophysical Research*, *117*, C08025. https://doi.org/10.1029/2012JC008141

Large, W. G., McWilliams, J. C., & Doney, S. C. (1994). Oceanic vertical mixing: A review and a model with a nonlocal boundary-layer parameterization. *Reviews of Geophysics*, *32*(4), 363–403.

Locarnini, R. A., Mishonov, A. V., Antonov, J. I., Boyer, T. P., Garcia, H. E., Baranova, O. K., et al. (2013). In S. Levitus & A. Mishonov (Eds.), *World ocean atlas 2013. Volume 1: Temperature* (pp. 1–40). NOAA Atlas NESDIS 73. Retrieved from https://repository.library.noaa.gov/view/noaa/14847

Mazur, A. K., Wahlin, A. K., & Kalen, O. (2019). The life cycle of small- to medium-sized icebergs in the Amundsen Sea Embayment. *Polar Research*, *38*. https://doi.org/10.33265/polar.v38.3313

Mazur, A. K., Wahlin, A. K., & Krezel, A. (2017). An object-based SAR image iceberg detection algorithm applied to the Amundsen Sea. *Remote Sensing of Environment*, *189*, 67–83.

Merino, N., le Sommer, J., Durand, G., Jourdain, N. C., Madec, G., Mathiot, P., & Tournadre, J. (2016). Antarctic icebergs melt over the Southern Ocean: Climatology and impact on sea ice. *Ocean Modelling*, *104*, 99–110.

Nakayama, Y., Menemenlis, D., Schodlok, M., & Rignot, E. (2017). Amundsen and Bellingshausen Seas simulation with optimized ocean, sea ice, and thermodynamic ice shelf model parameters. *Journal of Geophysical Research: Oceans*, *122*, 6180–6195. https://doi.org/10.1002/2016JC012538

Nakayama, Y., Menemenlis, D., Zhang, H., Schodlok, M., & Rignot, E. (2018). Origin of Circumpolar Deep Water intruding onto the Amundsen and Bellingshausen Sea continental shelves. *Nature Communications*, *9*(1), 3403. https://doi.org/10.1038/s41467-018-05813-1

Nakayama, Y., Schroder, M., & Hellmer, H. H. (2013). From circumpolar deep water to the glacial meltwater plume on the eastern Amundsen Shelf. *Deep-Sea Research Part I-Oceanographic Research Papers*, *77*, 50–62.

Nakayama, Y., Timmermann, R., Rodehacke, C. B., Schroder, M., & Hellmer, H. H. (2014). Modeling the spreading of glacial meltwater from the Amundsen and Bellingshausen Seas. *Geophysical Research Letters*, *41*, 7942–7949. https://doi.org/10.1002/2014GL061600

Nakayama, Y., Timmermann, R., Schröder, M., & Hellmer, H. H. (2014). On the difficulty of modeling Circumpolar Deep Water intrusions onto the Amundsen Sea continental shelf. *Ocean Modelling*, *84*, 26–34. https://doi.org/10.1016/j.ocemod.2014.09.007

Nihashi, S., & Ohshima, K. I. (2015). Circumpolar mapping of Antarctic coastal polynyas and landfast sea ice: Relationship and variability. *Journal of Climate*, *28*(9), 3650–3670. https://doi.org/10.1175/JCLI-D-14-00369.1

Paolo, F. S., Fricker, H. A., & Padman, L. (2015). Volume loss from Antarctic ice shelves is accelerating. *Science*, *348*(6232), 327–331.

Petty, A. A., Tsamados, M. C., & Kurtz, N. T. (2017). Atmospheric form drag coefficients over Arctic sea ice using remotely sensed ice topography data, spring 2009–2015. *Journal of Geophysical Research: Earth Surface*, *122*, 1472–1490. https://doi.org/10.1002/2017JF004209

Randall-Goodwin, E., Meredith, M. P., Jenkins, A., Yager, P. L., Sherrell, R. M., Abrahamsen, E. P., et al. (2015). Freshwater distributions and water mass structure in the Amundsen Sea Polynya region, Antarctica. *Elementa-Science of the Anthropocene*, *3*.

Regan, H. C., Holland, P. R., Meredith, M. P., & Pike, J. (2018). Sources, variability and fate of freshwater in the Bellingshausen Sea, Antarctica. *Deep-Sea Research Part I-Oceanographic Research Papers*, *133*, 59–71.

Rignot, E., Jacobs, S., Mouginot, J., & Scheuchl, B. (2013). Ice-shelf melting around Antarctica. *Science*, *341*(6143), 266–270.

Rye, C. D., Naveira Garabato, A. C., Holland, P. R., Meredith, M. P., George Nurser, A. J., Hughes, C. W., et al. (2014). Rapid sea-level rise along the Antarctic margins in response to increased glacial discharge. *Nature Geoscience*, *7*(10), 732–735. https://doi.org/10.1038/ngeo2230

Shepherd, A., Ivins, E., Rignot, E., Smith, B., van den Broeke, M., Velicogna, I., et al. (2018). Mass balance of the Antarctic Ice Sheet from 1992 to 2017. *Nature*, *558*, 219–222.

Shepherd, A., Wingham, D., & Rignot, E. (2004). Warm ocean is eroding West Antarctic Ice Sheet. *Geophysical Research Letters*, *31*, L23402. https://doi.org/10.1029/2004GL021106

Snow, K., Goldberg, D. N., Holland, P. R., Jordan, J. R., Arthern, R. J., & Jenkins, A. (2017). The response of ice sheets to climate variability. *Geophysical Research Letters*, *44*, 11,878–11,885. https://doi.org/10.1002/2017GL075745

Steig, E. J., Ding, Q., Battisti, D., & Jenkins, A. (2012). Tropical forcing of Circumpolar Deep Water inflow and outlet glacier thinning in the Amundsen Sea Embayment, West Antarctica. *Annals of Glaciology*, *53*(60), 19–28. https://doi.org/10.3189/2012AoG60A110

St-Laurent, P., Klinck, J. M., & Dinniman, M. S. (2015). Impact of local winter cooling on the melt of Pine Island Glacier, Antarctica. *Journal of Geophysical Research: Oceans*, *120*, 6718–6732. https://doi.org/10.1002/2015JC010709

St-Laurent, P., Yager, P. L., Sherrell, R. M., Stammerjohn, S. E., & Dinniman, M. S. (2017). Pathways and supply of dissolved iron in the Amundsen Sea (Antarctica). *Journal of Geophysical Research: Oceans*, *122*, 7135–7162. https://doi.org/10.1002/2017JC013162

Thoma, M., Jenkins, A., Holland, D., & Jacobs, S. (2008). Modelling Circumpolar Deep Water intrusions on the Amundsen Sea continental shelf, Antarctica. *Geophysical Research Letters*, *35*, L18602. https://doi.org/10.1029/2008GL034939

Walker, D. P., Brandon, M. A., Jenkins, A., Allen, J. T., Dowdeswell, J. A., & Evans, J. (2007). Oceanic heat transport onto the Amundsen Sea shelf through a submarine glacial trough. *Geophysical Research Letters*, *34*, L02602. https://doi.org/10.1029/2006GL028154

Walker, D. P., Jenkins, A., Assmann, K. M., Shoosmith, D. R., & Brandon, M. A. (2013). Oceanographic observations at the shelf break of the Amundsen Sea, Antarctica. *Journal of Geophysical Research: Oceans*, *118*, 2906–2918. https://doi.org/10.1002/jgrc.20212

Webber, B. G. M., Heywood, K. J., Stevens, D. P., Dutrieux, P., Abrahamsen, E. P., Jenkins, A., et al. (2017). Mechanisms driving variability in the ocean forcing of Pine Island Glacier. *Nature Communications*, *8*(1), 14507. https://doi.org/10.1038/ncomms14507

Worby, A. P., Geiger, C. A., Paget, M. J., van Woert, M. L., Ackley, S. F., & DeLiberty, T. L. (2008). Thickness distribution of Antarctic sea ice. *Journal of Geophysical Research*, *113*, C05S92. https://doi.org/10.1029/2007JC004254

Zweng, M. M., Reagan, J. R., Antonov, J. I., Locarnini, R. A., Mishonov, A. V., Boyer, T. P., et al. (2013). In S. Levitus & A. Mishonov (Eds.), *World ocean atlas 2013. Volume 2: Salinity* (pp. 1–39). NOAA Atlas NESDIS 74. Retrieved from https://repository.library.noaa.gov/view/noaa/14848